HHS Public Access

Author manuscript

Nat Struct Mol Biol. Author manuscript; available in PMC 2013 November 01.

Published in final edited form as:

Nat Struct Mol Biol. 2013 May ; 20(5): 628–633. doi:10.1038/nsmb.2554.

Conformational selection of translation initiation factor 3 signals proper substrate selection

Margaret M. Elvekrog[1,2] and **Ruben L. Gonzalez Jr.**[1]

[1]Department of Chemistry, Columbia University, New York, NY, USA

Abstract

During translation, initiation factor (IF) 3 binds to the small, 30S, ribosomal subunit and regulates the fidelity with which the initiator tRNA and mRNA start codon substrates are selected into the 30S initiation complex (30S IC). The molecular mechanism through which IF3 promotes recognition and signaling of correct substrate selection, however, remains poorly defined. Using single-molecule fluorescence resonance energy transfer, here we show that 30S IC-bound *Escherichia coli* IF3 exists in a dynamic equilibrium between at least three conformations. We have found that recognition of a proper anticodon-codon interaction between initiator tRNA and the start codon within a completely assembled 30S IC selectively shifts this equilibrium towards a single IF3 conformation. Our results strongly support a conformational selection model in which the conformation of IF3 that is selectively stabilized within a completely and correctly assembled 30S IC facilitates further progress along the initiation pathway.

Translation initiation, the rate-limiting step of protein synthesis and a major regulatory checkpoint in gene expression[1], involves a multistep, IF-mediated assembly of a 70S ribosomal initiation complex (70S IC) that contains an initiator *N*-formylmethionyl-transfer RNA (fMet-tRNA^{fMet}) and a messenger RNA (mRNA) start codon within the P (peptidyl-tRNA binding) site of the 70S IC (Fig. 1A)[1]. The accuracy of fMet-tRNA^{fMet} and start codon selection is critical, as selection of an elongator aminoacyl-tRNA (aa-tRNA) or a non-canonical start codon during 70S IC assembly can result in proteins harboring an incorrect N-terminal amino acid or in translation of a frameshifted mRNA. The fidelity of translation initiation is primarily established through the cooperative biochemical activities of three essential IFs: IF1, IF2, and IF3 (ref. 1). Extensive biochemical studies suggest that IF3 plays a negative regulatory role in ensuring the accuracy of translation initiation by uniformly destabilizing the binding of all tRNAs at the 30S IC P site[2] and by selectively inhibiting the joining of 50S subunits onto 30S ICs carrying elongator aa-tRNAs[2–4] or carrying an fMet-tRNA^{fMet} containing mismatched base pairs to a non-canonical start codon[5]. Despite these biochemical studies, however, a structure-based understanding of how IF3 recognizes and

Correspondence should be addressed to R.L.G. (rlg2118@columbia.edu).

[2]Present address: Department of Biochemistry and Biophysics, University of California, San Francisco, San Francisco, CA, USA

AUTHOR CONTRIBUTIONS

M.M.E. and R.L.G. contributed to the experimental design and writing of the manuscript. M.M.E. performed the experiments and carried out data analysis.

signals fMet-tRNA^{fMet} and start codon selection within the 30S IC in order to regulate further progress along the initiation pathway remains elusive.

IF3 is comprised of globular N-terminal and C-terminal domains (designated the NTD and CTD, respectively) that are connected *via* a flexible interdomain linker of highly conserved length and amino acid character[6] that enables IF3 to dynamically sample a broad range of interdomain conformations when free in solution (Fig. 1B)[7]. Whether 30S IC-bound IF3 exhibits similar conformational dynamics and whether these dynamics play a role in the fidelity function of IF3 within the 30S IC, however, remain unknown. Unfortunately, high-resolution structural information on the 30S IC is still lacking and, suggestively, attempts to localize IF3's binding site on the 30S IC have come to conflicting conclusions, particularly regarding the placement of IF3's NTD on the 30S IC[8–10]. At least one of the proposed IF3 binding sites is expected to sterically block formation of one of the key intersubunit bridges that connect the two ribosomal subunits within a 70S IC, thereby providing an attractive structural model for IF3's subunit anti-association activity[8,9]. On their own, however, structural models such as this fail to account for the selective relaxation of IF3's subunit anti-association activity upon correct substrate selection, as an fMet-tRNA^{fMet}- and start codon-dependent repositioning of IF3 on the 30S IC and/or dissociation of IF3 from the 30S IC[2,11] would be required to facilitate access to the 30S IC intersubunit bridge components that are otherwise blocked by IF3.

To determine whether IF3 is conformationally dynamic on the 30S IC and investigate whether these dynamics play a role in the fMet-tRNA^{fMet}- and start codon-dependent relaxation of IF3's subunit anti-association activity, we developed an intramolecular IF3 fluorescence resonance energy transfer (FRET) signal that reports on relative distance changes between IF3's NTD and CTD. Using single-molecule FRET (smFRET), we have discovered that 30S IC-bound IF3 samples and interconverts between at least three distinct FRET states, demonstrating that IF3 exists in a conformational equilibrium on the 30S IC. By conducting smFRET experiments on a series of 30S ICs, we show that the presence of either or both of the other IFs, IF1 and IF2, on the 30S IC can modulate the conformational equilibrium of 30S IC-bound IF3. Most importantly, however, we demonstrate that the presence and identities of the tRNA and codon that are positioned within the P site of the 30S IC can also modulate the conformational equilibrium of 30S IC-bound IF3 such that the presence of an initiator tRNA and start codon uniquely shift the equilibrium toward a single conformation of IF3. Integrated with the available biochemical data, we use our results to propose a conformational selection model in which the conformation of IF3 that is uniquely stabilized within a completely and correctly assembled 30S IC facilitates further progress along the initiation pathway, whereas alternative conformations of IF3 are inhibitory.

RESULTS

Development of a functional, dual fluorescently labeled IF3

Labeling of a two cysteine-containing IF3 mutant carrying one cysteine at its NTD and one cysteine at its CTD with Cy3 FRET donor and Cy5 FRET acceptor fluorophores and subsequent purification generated a dual Cy3-Cy5 labeled IF3 (IF3$_{C65S\ S38C\ K97C}$(Cy3-Cy5), hereafter IF3(Cy3-Cy5)) (Fig. 1B, Supplementary Fig. 1) that retained near-wild-type

biochemical function (Supplementary Fig. 2). 30S ICs carrying IF3(Cy3-Cy5) were assembled on 5′-biotinylated mRNAs, tethered to the polyethylene glycol-passivated and streptavidin-derivatized surface of a quartz microfluidic flowcell, and imaged at single-molecule resolution using a total internal reflection fluorescence (TIRF) microscope operating at an acquisition rate of 10 frames sec^{-1} (ref. 12). Control experiments demonstrated that, under our experimental conditions, 80–95% of individual, surface-localized IF3(Cy3-Cy5)s were bound to the flowcell surface *via* their interaction with a 30S IC carrying a biotinylated mRNA (Supplementary Fig. 3). For further details regarding sample preparation, TIRF imaging, control experiments, and data analysis please see the Supplementary Note.

30S IC-bound IF3 is conformationally dynamic

Initial experiments were designed to probe the conformation of IF3 bound to a 30S subunit in the absence of the other IFs and tRNA ($^{30S}IC^{-tRNA}_{-1/-2}$, where the −tRNA superscript and −1/−2 subscript denote the lack of a P-site tRNA and the lack of IF1 and IF2, respectively). The resulting smFRET efficiency (E_{FRET}) *versus* time trajectories sampled three distinct FRET states centered at E_{FRET} values of 0.23 ± 0.01, 0.42 ± 0.01, and 0.87 ± 0.01, with 29.9 ± 8.6% of the trajectories exhibiting fluctuations between at least two FRET states prior to photobleaching and 70.1 ± 17.3% of the trajectories sampling only one of these FRET states prior to photobleaching (Fig. 2A and Supplementary Fig. 4). Assuming rapid, isotropic tumbling of one or both fluorophore transition dipoles and a Förster radius of ~55 Å for the Cy3-Cy5 FRET pair[12,13], we interpret the E_{FRET} values of 0.23, 0.42, and 0.87 (Supplementary Table 1) as corresponding to interdomain distances of ~67 Å, ~58 Å, and ~40 Å, respectively. Notably, this range of distances is consistent with the interdomain distances accessible to IF3 when free in solution (28–65 Å)[7]. Hereafter, we will refer to the conformations of the 30S IC-bound IF3 associated with each of these E_{FRET} values/distances as: extended ($IF3_{ext}$, 0.23/~67 Å), intermediate ($IF3_{int}$, 0.42/~58 Å), and compact ($IF3_{cpt}$, 0.87/~40 Å). Thermodynamic and kinetic analysis of the trajectories revealed equilibrium fractional occupancies of 55 ± 9%, 40 ± 10%, and 6 ± 2% for $IF3_{ext}$, $IF3_{int}$, and $IF3_{cpt}$, respectively (Supplementary Table 2) and estimated rates of interconversions between the three IF3 conformations ranging between 0.002–0.11 sec^{-1} (Supplementary Table 3). Interpreted within the context of previously reported *in vitro* subunit joining experiments demonstrating that 30S analogous to $^{30S}IC^{-tRNA}_{-1/-2}$ are substantially inhibited in their ability to undergo subunit joining[4], these data suggest that $IF3_{ext}$ and $IF3_{int}$ represent conformations of IF3 that are not conducive to rapid 50S subunit joining.

It is unlikely that the interdomain dynamics of IF3 which we observe here arise from a scenario in which one IF3 domain is tightly bound to the 30S IC while the other IF3 domain remains free in solution, undergoing restricted diffusion via the interdomain linker. Dynamic exchange between different interdomain conformations of IF3 involving such restricted diffusion of a free IF3 domain would be expected to occur with rates that are 7–11 orders of magnitude faster than our estimated rates of interconversions between $IF3_{ext}$, $IF3_{int}$, and $IF3_{cpt}$[14]. Instead, we propose a scenario in which both IF3 domains can bind to the 30S IC and exchange between different interdomain conformations due either to: (i) active

repositioning of one or both IF3 domains amongst several binding sites on the 30S IC; (ii) passive changes in the distance between the two IF3 domains resulting from dynamic rearrangements of the 30S IC; or (iii) a combination of (i) and (ii). To test whether IF3 is actively or passively participating in the observed dynamics, we constructed an IF3(Cy3-Cy5) mutant that carries a single tyrosine to asparagine substitution at amino acid position 75 (Y75N) within the interdomain linker ($IF3_{C65S\ S38C\ K97C\ Y75N}$(Cy3-Cy5), hereafter $IF3_{Y75N}$(Cy3-Cy5))[15]. Previous studies have shown that the Y75N mutation perturbs the fMet-$tRNA^{fMet}$ and start codon selection activity of IF3, but doesn't affect its ability to bind to 30S subunits[15], biochemical properties that were recapitulated by our $IF3_{Y75N}$(Cy3-Cy5) construct (Supplementary Fig. 2). Comparison of smFRET data recorded using IF3(Cy3-Cy5) and $IF3_{Y75N}$(Cy3-Cy5) on otherwise identical 30S ICs and under otherwise identical experimental conditions reveals that the Y75N mutation appreciably alters the conformational equilibrium of IF3 (Supplementary Figs. 3 and 5). The observation that a substitution mutation within the interdomain linker of IF3 can alter the dynamics we observe here demonstrates that IF3 is playing an active role in modulating the conformational equilibrium between $IF3_{ext}$, $IF3_{int}$, and $IF3_{cpt}$, regardless of whether these dynamics originate from repositioning of IF3 domains on a static 30S IC and/or from structural rearrangements of the 30S IC itself. Furthermore, the fact that $IF3_{Y75N}$(Cy3-Cy5) exhibits impaired fMet-$tRNA^{fMet}$ and start codon selection activity (Supplementary Fig. 2) suggests a functional link between the dynamics we observe here and the fidelity function of IF3.

IF1 and IF2 modulate the conformational equilibrium of IF3

Because IF1 amplifies and IF2 counteracts the tRNA dissociation and subunit anti-association activities of IF3 during translation initiation[2], we next investigated the effects of IF1 and IF2 on the conformational dynamics of 30S IC-bound IF3 by assembling and imaging 30S ICs in the presence of IF1 ($30S\,IC_{-2}^{-tRNA}$), IF2 ($30S\,IC_{-1}^{-tRNA}$), and both IF1 and IF2 (30S IC^{-tRNA}) (Fig. 2B). 30S ICs carrying IF1 and/or IF2 were imaged under saturating, 1 μM concentrations of each of these components. Relative to $30S\,IC_{-1/-2}^{-tRNA}$, the presence of IF1 slightly shifts the conformational equilibrium of $30S\,IC_{-2}^{-tRNA}$-bound IF3 away from $IF3_{ext}$ and $IF3_{cpt}$ and towards $IF3_{int}$, yielding fractional occupancies of 45 ± 3% ($IF3_{ext}$), 53 ± 3% ($IF3_{int}$), and 3 ± 1% ($IF3_{cpt}$) (Fig. 2B Supplementary Table 2). In contrast, relative to $30S\,IC_{-1/-2}^{-tRNA}$, the presence of IF2 markedly shifts the conformational equilibrium of $30S\,IC_{-1}^{-tRNA}$-bound IF3 away from $IF3_{ext}$ and $IF3_{int}$ and towards $IF3_{cpt}$, yielding fractional occupancies of 23 ± 17% ($IF3_{ext}$), 11 ± 4% ($IF3_{int}$), and 66 ± 17% ($IF3_{cpt}$) (Fig. 2B, Supplementary Table 2). Strikingly, the effect of IF2 on the conformational equilibrium of 30S IC-bound IF3 is almost completely suppressed when IF1 is included together with IF2 in 30S IC^{-tRNA} (Fig. 2B, Supplementary Table 2). Thus, in the most physiologically relevant scenario in which all three IFs are present on the 30S IC[16], the conformational equilibrium of 30S IC^{-tRNA}-bound IF3 almost exclusively favors $IF3_{ext}$ and $IF3_{int}$, yielding fractional occupancies of 57 ± 7% ($IF3_{ext}$), 42 ± 6% ($IF3_{int}$), and only 2 ± 1% ($IF3_{cpt}$) (Fig. 2B, Supplementary Table 2) and transition rates that are similar to those observed in $30S\,IC_{-1/-2}^{-tRNA}$ (Supplementary Table 3).

fMet-tRNA^{fMet} shifts the equilibrium towards IF3$_{cpt}$

A completely and correctly assembled 30S IC that is primed for rapid 50S subunit docking contains an fMet-tRNA^{fMet} that is correctly base paired to a start codon within the 30S IC P site. Driven by this, we next assembled and imaged a 30S IC containing IF1, IF2, IF3(Cy3-Cy5), and fMet-tRNA^{fMet} on an mRNA containing an AUG start codon (30S IC^{fMet}) using saturating, 1 μM concentrations of IF1, IF2, and fMet-tRNA^{fMet}. Notably, the average number of surface-tethered, 30S IC^{fMet}-bound IF3(Cy3-Cy5) molecules that were observed per field-of-view did not vary appreciably relative to the number of surface-tethered, 30S IC-bound IF3(Cy3-Cy5) molecules that were observed in any of the other identically prepared and imaged 30S ICs we have studied. Thus, the presence of an fMet-tRNA^{fMet} that is correctly base paired to a start codon within the P site of 30S IC^{fMet}, at least within the context of the mRNA used here, does not seem to trigger rapid dissociation of IF3 from the 30S IC within the timescale of our experiments (~10 min)[3,5,17]. Instead we find that, relative to 30S IC^{-tRNA}, the presence of an fMet-tRNA^{fMet} that is correctly base paired to an AUG start codon within 30S IC^{fMet} dramatically shifts the conformational equilibrium of IF3 away from IF3$_{ext}$ and IF3$_{int}$ and towards IF3$_{cpt}$ (Fig. 3), yielding fractional occupancies of 15 ± 13% (IF3$_{ext}$), 17 ± 7% (IF3$_{int}$), and 68 ± 17% (IF3$_{cpt}$) (Supplementary Table 2). This equilibrium shift seems to be primarily driven by the destabilization of IF3$_{ext}$ and IF3$_{int}$, as evidenced by the large increases in the estimated rates of IF3$_{ext}$→IF3$_{cpt}$ and IF3$_{int}$→IF3$_{cpt}$ transitions in 30S IC^{fMet} relative to 30S IC^{-tRNA} (Supplementary Table 3). Based on these results, we hypothesized that the observed shift in the conformational equilibrium of 30S IC-bound IF3 towards IF3$_{cpt}$ in 30S IC^{fMet} relative to 30S IC^{-tRNA} forms the molecular and structural basis for signaling fMet-tRNA^{fMet} and start codon selection within the 30S IC and the associated relaxation of IF3's subunit anti-association activity. Consistent with this hypothesis, previously reported *in vitro* 50S subunit joining experiments demonstrate that 30S ICs analogous to 30S IC^{fMet} undergo rapid 50S subunit joining relative to 30S ICs analogous to 30S IC^{-tRNA} (ref. 4), suggesting that IF3$_{cpt}$ represents a conformation of IF3 that is conducive for rapid 50S subunit joining. In the context of this hypothesis, IF3$_{ext}$ and IF3$_{int}$ not only represent conformations of IF3 that are not conducive to 50S subunit joining, as was discussed above, but also conformations of IF3 that prevent IF3 from populating IF3$_{cpt}$, and, consequently, from undergoing rapid 50S subunit joining, until the 30S IC has properly selected an fMet-tRNA^{fMet} and the start codon.

The shift towards IF3$_{cpt}$ requires fMet-tRNA^{fMet} and an AUG codon

If the hypothesis outlined in the previous paragraph is correct, then we would expect the shift in the conformational equilibrium of IF3 to depend on the identity of the tRNA and/or codon within the 30S IC P site, since signaling of proper substrate selection and the associated rapid 50S subunit joining occur only within 30S ICs specifically carrying an fMet-tRNA^{fMet} that is properly base paired to a start codon. Thus, to further test our hypothesis, we assembled and imaged complete 30S ICs in which the identities of the tRNA and/or the codon at the P site were varied. In line with our hypothesis, 30S ICs assembled and imaged using saturating, 1 μM concentrations of either Phe-tRNA^{Phe} or Lys-tRNA^{Lys} and an AUG start codon at the P site (30S IC^{Phe} and 30S IC^{Lys}, respectively) did not undergo the shift in the conformational equilibrium of IF3 towards IF3$_{cpt}$ relative to 30S

IC^{-tRNA} that is observed for 30S IC^{fMet} relative to 30S IC^{-tRNA} (Fig. 3). Instead, the fractional occupancies of $IF3_{ext}$, $IF3_{int}$, and $IF3_{cpt}$ within 30S IC^{Phe} and 30S IC^{Lys} are comparable to those observed within 30S IC^{-tRNA}, despite the presence of saturating concentrations of Phe-$tRNA^{Phe}$ or Lys-$tRNA^{Lys}$ (Fig. 3 and Supplementary Table 2). Comparison of 30S IC^{-tRNA}, 30S IC^{fMet}, 30S IC^{Phe}, and 30S IC^{Lys} demonstrates that the shift in the conformational equilibrium of IF3 towards $IF3_{cpt}$ depends not only on the presence of an aa-tRNA at the 30S IC P site, but also on the identity of that aa-tRNA. Nevertheless, by altering the identity of the aa-tRNA, but not the AUG start codon, the P sites of 30S IC^{Phe} and 30S IC^{Lys} do not just contain incorrectly selected elongator aa-tRNAs, but also mismatched GAA-AUG and UUU-AUG anticodon-codon interactions, respectively. Thus, the failure of 30S IC^{Phe} and 30S IC^{Lys} to exhibit a shift in the conformational equilibrium of IF3 towards $IF3_{cpt}$ relative to 30S IC^{-tRNA} could potentially be due to the presence of the elongator aa-tRNA and/or the mismatched anticodon-codon interaction within the 30S IC P site.

In order to separate the effects that the identity of the aa-tRNA and the nature of the anticodon-codon base-pairing interactions have on the conformational equilibrium of IF3, we imaged completely assembled 30S ICs whose P sites contained either Phe-$tRNA^{Phe}$ at a UUC codon that is cognate for Phe-$tRNA^{Phe}$ (30S $IC^{Phe,UUC}$) or fMet-$tRNA^{fMet}$ at an AUU codon that is near-cognate for fMet-$tRNA^{fMet}$ (30S $IC^{fMet,AUU}$) using saturating, 1 μM concentrations of Phe-$tRNA^{Phe}$ or fMet-$tRNA^{fMet}$, respectively. Despite the Watson-Crick complementarity of the anticodon-codon interaction in 30S $IC^{Phe,UUC}$, IF3 again exhibits thermodynamic and kinetic behavior that is comparable to that observed for IF3 within 30S IC^{-tRNA}, despite the presence of saturating concentrations of Phe-$tRNA^{Phe}$ (Fig. 3 and Supplementary Table 2). Similarly, in the presence of a partially mismatched anticodon-codon interaction in 30S $IC^{fMet,AUU}$, IF3 exhibits thermodynamic and kinetic behavior that is comparable to 30S IC^{-tRNA}, despite the presence of saturating concentrations of fMet-$tRNA^{fMet}$ (Fig. 3 and Supplementary Table 2).

DISCUSSION

Taken together, the results obtained with 30S IC^{Phe}, 30S IC^{Lys}, 30S $IC^{Phe,UUC}$, and 30S $IC^{fMet,AUU}$ suggest that, relative to 30S IC^{-tRNA}, the shift in the conformational equilibrium of IF3 towards $IF3_{cpt}$ is dependent on the specific presence of an fMet-$tRNA^{fMet}$ at the 30S IC P site as well as proper base pairing between the fMet-$tRNA^{fMet}$ and a start codon at the P site; these are precisely the conditions under which extensive *in vitro* biochemical experiments have shown that the subunit anti-association activity of IF3 is relaxed and 50S subunit association to the 30S IC is accelerated[4]. Specifically, rapid kinetic experiments have shown that, within the context of a 30S IC containing all three IFs, the presence of an fMet-$tRNA^{fMet}$ and an AUG start codon increases the rate of 50S subunit joining by a factor of 1200 relative to a 30S IC lacking a P-site aa-tRNA[4], a factor of 400 relative to a 30S IC carrying a Phe-$tRNA^{Phe}$ that is mismatched to an AUG start codon[2], and a factor of 90 relative to a 30S IC carrying an fMet-$tRNA^{fMet}$ that is mismatched to a non-canonical start codon[5].

Integrating our current findings regarding the conformational dynamics of 30S IC-bound IF3 with the results of the biochemical studies described in the previous paragraph allows us to propose a structure-based mechanistic model for how IF3 recognizes and signals fMet-tRNA^{fMet} and start codon selection within the 30S IC in order to gate further progress along the initiation pathway. In our model, 30S IC-bound IF3 can sample at least three major conformations, IF3$_{ext}$, IF3$_{int}$, or IF3$_{cpt}$, whose thermodynamic stabilities respond dramatically to the composition of the 30S IC. In 30S ICs carrying all three IFs, but either lacking an aa-tRNA, carrying an elongator aa-tRNA, or carrying an fMet-tRNA^{fMet} that is mismatched to a non-canonical start codon within the 30S IC P site, the conformational equilibrium of IF3 is heavily shifted towards IF3$_{ext}$ and IF3$_{int}$: conformations of IF3 that are not conducive to rapid 50S subunit joining. Specific recognition of an fMet-tRNA^{fMet} that is properly base paired to a start codon within the P site of a 30S IC carrying all three IFs, in contrast, dramatically shifts the conformational equilibrium of IF3 towards IF3$_{cpt}$: a conformation of IF3 that signals proper substrate selection and is conducive to rapid 50S subunit joining. It is interesting to note that IF3 predominantly occupies IF3$_{cpt}$ in both the completely and correctly assembled 30S IC (i.e. 30S IC^{fMet}) as well as in the incompletely assembled 30S IC lacking IF1 and fMet-tRNA^{fMet} (i.e. $30S\,IC_{-1}^{-tRNA}$) (Figs. 2B and 3). Thus, in the absence of IF1 and fMet-tRNA^{fMet}, the presence of just IF2 on the 30S IC can shift IF3's conformational equilibrium towards IF3$_{cpt}$. This is intriguing in light of rapid kinetic data indicating that 50S subunit joining to a 30S IC that is analogous to $30S\,IC_{-1}^{-tRNA}$ is 145-fold slower than to a 30S IC that is analogous to 30S IC^{fMet} (ref. 3). Thus, although our model stipulates that IF3$_{cpt}$ is conducive for and permits rapid 50S subunit joining, it is likely that additional factors such as the presence of IF2 and fMet-tRNA^{fMet} on the 30S IC are required to actualize rapid 50S subunit joining[2,3]. Furthermore, the finding that IF3$_{cpt}$ is rarely sampled within 30S IC^{-tRNA} suggests that IF1 plays a key role in negatively regulating the conformational dynamics of IF3 such that 30S IC-bound IF3 does not significantly populate IF3$_{cpt}$ in the absence of fMet-tRNA^{fMet} that is correctly base paired to a start codon.

Although confirming our suspicions will have to wait until long-anticipated X-ray crystallographic structures of the 30S IC are solved, we suspect that IF3$_{cpt}$ is a conformation of the 30S IC-bound IF3 that exposes and/or optimally positions ribosomal RNA and/or ribosomal protein residues on the 30S IC that are critical for intersubunit bridge formation, thus enabling rapid and productive 50S subunit joining, while IF3$_{ext}$ and IF3$_{int}$ are conformations of the 30S IC-bound IF3 that occlude and/or misorient these residues, thereby blocking 50S subunit joining. In contrast with models in which a selective increase in the rate of spontaneous dissociation of IF3 from the 30S IC is required for productive 50S subunit joining[3] the model presented here predicts that efficient 50S subunit joining can occur on a completely and correctly assembled 30S IC that contains IF3. Indeed, preliminary smFRET data collected using a Cy3-labeled IF3 and a Cy5-labeled 50S subunit (labeled at ribosomal protein L9) reveal that the 50S subunit can rapidly and productively join to a completely and correctly assembled 30S IC containing IF3 that is presumably in the IF3$_{cpt}$ conformation (i.e. 30S IC^{fMet}) (Fig. 4). Nevertheless, our model (Fig. 5) and intermolecular 50S-IF3 smFRET data do not exclude the possibility that IF3 in the IF3$_{cpt}$ conformation is more weakly bound to the 30S IC than IF3 in the IF3$_{ext}$ and IF3$_{int}$ conformations such that

IF3 in the $IF3_{cpt}$ conformation is easily displaced from the 30S IC during or shortly after productive 50S subunit joining. Indeed kinetic measurements by Rodnina and co-workers[5] and Cooperman and co-workers[18] suggest that 50S subunit joining to the 30S IC is slightly faster than the rate of IF3 dissociation from the 30S IC. Given recent studies demonstrating that differences in the translation initiation region (TIR) of individual mRNAs, such as the sequence of the Shine-Dalgarno (SD) element and the length of the spacer between the SD element and the start codon, can influence the rate of 50S subunit joining to 30S ICs assembled on different mRNAs[5,17], it is possible that TIR-mediated regulation of the conformational equilibrium of 30S IC-bound IF3 will prove an effective mechanism for regulating the efficiency with which individual mRNAs are initiated and translated in the cell.

ONLINE METHODS

Sample preparation

E. coli ribosomes and translation factors were purified as previously described[20]. 5′-biotinylated mRNA with a sequence derived from the mRNA encoding gene product 32 from T4 bacteriophage was purchased from Dharmacon, Inc. See the Supplementary Note for details on the sequence of this mRNA. $tRNA^{fMet}$ was purchased from MP Biomedicals and $tRNA^{Phe}$ and $tRNA^{Lys}$ were purchased from Sigma. All tRNAs were aminoacylated and, in the case of $tRNA^{fMet}$, formylated as previously described[20].

The gene for *E. coli* IF3 was cloned into the pProEx-HTb plasmid vector (Invitrogen), which encodes a six-histidine (6×His) affinity purification tag and a TEV protease cleavage site at the N-terminal end of the gene encoding IF3. Mutagenesis of IF3 in the pProEx-HTb plasmid vector was performed using the QuickChange Site-Directed Mutagenesis System (Stratagene). DNA primers for mutagenesis were designed following the recommendations provided by the QuickChange Site-Directed Mutagenesis System and were purchased from Integrated DNA Technologies. No further purification of the DNA primers was performed. Using this approach, the single Cys65 in wild-type IF3 was mutagenized to Ser, Ser38 in the NTD was mutagenized to Cys, and Lys97 in the CTD was mutagenized to Cys, yielding a triple-mutant IF3 variant (IF3(C65S S38C K97C)). Note that the amino acid numbering for IF3 used in this study is based on wild-type *E. coli* IF3 numbering. Mutations were verified by DNA sequencing of the plasmid purified from an ampicillin-resistant clone (Genewiz). The pProEx-HTb plasmids encoding all of the IF3 variants used in this study were transformed into BL21-DE3 cells for protein overexpression and the overexpressed 6×His-tagged IF3 variants were purified using Ni^{2+}-nitrilotriacetic acid affinity purification, treated with TEV protease to remove the 6×His tags, and further purified using cation exchange chromatography. Further details regarding the cloning, overexpression, and purification of the IF3 variants used in this study can be found in reference 20. The N-terminus of the IF3 variants used in this study consists of a Gly-Ala-Met-Ala-Lys2 sequence, where Gly-Ala-Met-Ala denotes four non-wild-type amino acids resulting from the cloning strategy and Lys2 denotes the beginning of the wild-type *E. coli* IF3 sequence.

IF3(C65S S38C K97C) was labeled with Cy3- and Cy5-maleimide (GE Healthcare) following the manufacturer's recommendations. See Supplementary Note for further details.

The unlabeled, mono-labeled, and dual-labeled IF3(C65S S38C K97C) products were separated using a TSKgel Phenyl-5PW hydrophobic interaction chromatography (HIC) column (Tosoh Bioscience) that had been pre-equilibrated with HIC Buffer A (Supplementary Table 4). A 0–100% linear gradient of HIC Buffer B applied over 20 column volumes enabled separation of the various unlabeled and labeled IF3 species (Supplementary Fig. 1).

The biochemical activities of mutagenized and fluorescently labeled IF3(C65S S38C K97C) (IF3(Cy3-Cy5)) and IF3(C65S S38C K97C Y75N) was tested using a primer extension inhibition, or toeprinting, assay and a TIRF microscopy-based tRNA dissociation assay (Supplementary Fig. 2).

30S ICs for smFRET studies were prepared by incubating 1.8 μM 5′-biotinylated mRNA, 0.9 μM IF1, 0.9 μM IF2, 0.9 μM tRNA, 0.6 μM 30S subunits, and 0.6 μM IF3(Cy3-Cy5) at 37°C for 10 min in Tris-Polymix Buffer (Supplementary Table 4). 30S ICs were then aliquoted, flash frozen in liquid nitrogen, and stored at −80 °C until further use.

Total internal reflection fluorescence (TIRF) microscopy

30S ICs for imaging by TIRF microscopy were thawed, diluted to ~200 pM in Tris-Polymix Buffer (Supplementary Table 4), introduced into a microfluidic flowcell that had been passivated with a mixture of polyethylene glycol and biotinylated polyethylene glycol (PEG) and derivatized with streptavidin as previously described[21], and incubated at room temperature for 5 min. 30S ICs that failed to tether to the surface of the flowcell at the end of the 5 min incubation were removed by flushing the flowcell with Tris-Polymix Buffer containing an enzymatic oxygen scavenger system, a triplet state quencher cocktail, and, as specified in individual experiments, mixtures of IFs and aminoacyl-tRNAs (Supplementary Table 4).

A previously described, laboratory-built, wide-field, prism-based TIRF microscope[22] was used to image the flowcells containing the surface-tethered 30S ICs. Briefly, a diode-pumped, solid-state, 532 nm laser (CrystaLaser) operating at a power of 7 mW (measured just prior to striking the prism) was used to directly excite Cy3 and a diode-pumped, solid-state, 643 nm laser (CrystaLaser) operating at a power of 18 mW (measured just prior to striking the prism) was used to directly excite Cy5. Fluorescence emission from Cy3 and/or Cy5 was collected through a high numerical aperture objective (Nikon), wavelength separated into individual Cy3 and Cy5 fields-of-view using a Dual-View simultaneous imaging system (Photometrics, Inc.), and simultaneously imaged using the two halves of a back-thinned, 512 x 512 pixel electron-multiplying charged-coupled device (EMCCD) camera (Cascade II 512:B; Photometrics, Inc.) operating with 2 x 2 pixel binning and a frame rate of 10 frames sec^{-1}.

200–400 spatially well-separated 30S ICs were imaged within a 60 x 120 μm^2 field-of-view. Direct excitation of Cy5 using the 643 nm laser during the first frame of each movie was used to record the spatial location of each Cy5 fluorophore in the field-of-view. The 643 nm laser was subsequently switched off and, simultaneously, the 532 nm laser was switched on in order to directly excite Cy3 and perform smFRET imaging starting with the second frame

of each movie. Imaging continued until >95% of the Cy3 fluorophores had photobleached. Three independent datasets consisting of 12–15 movies each were collected on separate days using independently prepared samples and microfluidic devices for each 30S IC.

smFRET data analysis

Generation and selection of single-molecule E_{FRET} *versus* time trajectories from each movie was performed as previously described[19,21,23]. Briefly, the first frame of each movie, which was collected using direct excitation of Cy5 with a 643 nm laser, was used to identify single, diffraction-limited Cy5 spots. The locations of these spots were transferred to the Cy3 field-of-view in order to align the Cy5 field-of-view with the subsequent 532 nm-directly excited Cy3 field-of-view. The aligned Cy3- and Cy5 fields-of-view were used to identify pairs of Cy3 and Cy5 spots corresponding to single, surface-tethered, 30S ICs carrying dual Cy3-Cy5 labeled IF3s and MetaMorph (Molecular Devices), Excel (Microsoft), Origin (OriginLab Corporation), or Matlab (The MathWorks) were used to plot Cy3- and Cy5 intensity *versus* time trajectories for each IF3. Trajectories exhibiting: (i) time-averaged Cy3 and Cy5 intensity values characteristic of single Cy3 and Cy5 fluorophores, respectively, as determined by visual inspection; (ii) single-step photobleaching of Cy3 and/or Cy5 fluorophores as determined by visual inspection; (iii) anticorrelated changes in Cy3 and Cy5 intensities as determined by visual inspection and (iv) Cy5 fluorescence lasting longer than one second prior to photobleaching as determined by visual inspection were kept for further analysis (see Fig. 2A for representative Cy3- and Cy5 *versus* time trajectories). In addition to these selection criteria, trajectories in which FRET could not be confirmed due to the simultaneous, single-step drop of both Cy3 and Cy5 intensities to baseline prior to undergoing an anticorrelated change in Cy3 and Cy5 intensities (<10 % of the total number of trajectories per independently collected dataset) were omitted from further analysis. Each of the Cy3- and Cy5 *versus* time trajectories selected for further analysis was baseline corrected by subtracting the average EMCCD readout over the last ten Cy3 time points (i.e. after photobleaching of the Cy3 fluorophore) from each Cy3 time point and subtracting the average EMCCD readout over the last ten Cy5 time points (i.e. after photobleaching of the Cy5 fluorophore) from each Cy5 time point. In addition, each Cy5 time point was corrected for bleed-through of Cy3 intensity into the Cy5 field-of-view, which arises from the imperfect performance of emission filters, by subtracting 7% of the total Cy3 intensity (i.e. the experimentally determined average amount of Cy3 intensity that bleeds through into the Cy5 field-of-view in our TIRF microscope system) at each time point from the Cy5 intensity at the same time point. Each pair of baseline- and bleed-through-corrected Cy3- and Cy5 *versus* time trajectories were converted to a single, raw E_{FRET} *versus* time trajectory using the equation $E_{FRET}=I_{Cy5}/(I_{Cy3} + I_{Cy5})$, where E_{FRET} is the FRET efficiency at each time point and I_{Cy3} and I_{Cy5} are the baseline- and bleed-through-corrected Cy3 and Cy5 intensities at each time point, respectively. The raw E_{FRET} *versus* time trajectories were idealized by hidden Markov modeling using the vbFRET software package[24] and further analyzed as described in Fig. 2 and Supplementary Tables 2–4.

Supplementary Material

Refer to Web version on PubMed Central for supplementary material.

Acknowledgments

We would like to thank M. A. Gawinowicz for performing trypsin digestion and MALDI-TOF mass spectrometry analysis of IF3(Cy3-Cy5), D. MacDougall for assistance with protein purification, and J.W. van de Meent for assistance with smFRET data analysis. We also thank members of the Gonzalez research group, especially D. MacDougall, J. Wang, K. Caban, and C. Kinz-Thompson for discussions and comments on the manuscript. Financial support for this work was provided by Career Award in the Biomedical Sciences #1004856 from the Burroughs Wellcome Fund (R.L.G.), Research Project Grant #GM084288 from the U. S. National Institutes of Health (R.L.G.), and Molecular Biophysics Training Grant #T32GM008281 from the U. S. National Institutes of Health (M.M.E.).

References

1. Laursen BS, Sorensen HP, Mortensen KK, Sperling-Petersen HU. Initiation of protein synthesis in bacteria. Microbiol Mol Biol Rev. 2005; 69:101–23. [PubMed: 15755955]
2. Antoun A, Pavlov MY, Lovmar M, Ehrenberg M. How initiation factors maximize the accuracy of tRNA selection in initiation of bacterial protein synthesis. Mol Cell. 2006; 23:183–93. [PubMed: 16857585]
3. Antoun A, Pavlov MY, Lovmar M, Ehrenberg M. How initiation factors tune the rate of initiation of protein synthesis in bacteria. EMBO J. 2006; 25:2539–50. [PubMed: 16724118]
4. Antoun A, Pavlov MY, Tenson T, Ehrenberg M. Ribosome formation from subunits studied by stopped-flow and Rayleigh light scattering. Biol Proced Online. 2004; 6:35–54. [PubMed: 15103398]
5. Milon P, Konevega AL, Gualerzi CO, Rodnina MV. Kinetic checkpoint at a late step in translation initiation. Mol Cell. 2008; 30:712–20. [PubMed: 18570874]
6. de Cock E, Springer M, Dardel F. The interdomain linker of Escherichia coli initiation factor IF3: a possible trigger of translation initiation specificity. Mol Microbiol. 1999; 32:193–202. [PubMed: 10216872]
7. Moreau M, et al. Heteronuclear NMR studies of E. coli translation initiation factor IF3. Evidence that the inter-domain region is disordered in solution. J Mol Biol. 1997; 266:15–22. [PubMed: 9054966]
8. Dallas A, Noller HF. Interaction of translation initiation factor 3 with the 30S ribosomal subunit. Mol Cell. 2001; 8:855–64. [PubMed: 11684020]
9. Julian P, et al. The Cryo-EM Structure of a Complete 30S Translation Initiation Complex from Escherichia coli. PLoS Biol. 2011; 9:e1001095. [PubMed: 21750663]
10. McCutcheon JP, et al. Location of translational initiation factor IF3 on the small ribosomal subunit. Proc Natl Acad Sci U S A. 1999; 96:4301–6. [PubMed: 10200257]
11. Fabbretti A, et al. The real-time path of translation factor IF3 onto and off the ribosome. Mol Cell. 2007; 25:285–96. [PubMed: 17244535]
12. Murphy MC, Rasnik I, Cheng W, Lohman TM, Ha T. Probing single-stranded DNA conformational flexibility using fluorescence spectroscopy. Biophys J. 2004; 86:2530–7. [PubMed: 15041689]
13. Bastiaens PI, Jovin TM. Microspectroscopic imaging tracks the intracellular processing of a signal transduction protein: fluorescent-labeled protein kinase C beta I. Proc Natl Acad Sci U S A. 1996; 93:8407–12. [PubMed: 8710884]
14. Adcock SA, McCammon JA. Molecular dynamics: survey of methods for simulating the activity of proteins. Chem Rev. 2006; 106:1589–615. [PubMed: 16683746]
15. Maar D, et al. A single mutation in the IF3 N-terminal domain perturbs the fidelity of translation initiation at three levels. J Mol Biol. 2008; 383:937–44. [PubMed: 18805426]
16. Howe JG, Hershey JW. Initiation factor and ribosome levels are coordinately controlled in Escherichia coli growing at different rates. J Biol Chem. 1983; 258:1954–9. [PubMed: 6337147]
17. Milon P, Maracci C, Filonava L, Gualerzi CO, Rodnina MV. Real-time assembly landscape of bacterial 30S translation initiation complex. Nat Struct Mol Biol. 2012; 19:609–15. [PubMed: 22562136]

18. Grigoriadou C, Marzi S, Pan D, Gualerzi CO, Cooperman BS. The translational fidelity function of IF3 during transition from the 30 S initiation complex to the 70 S initiation complex. J Mol Biol. 2007; 373:551–61. [PubMed: 17868695]
19. Fei J, et al. Allosteric collaboration between elongation factor G and the ribosomal L1 stalk directs tRNA movements during translation. Proc Natl Acad Sci U S A. 2009; 106:15702–7. [PubMed: 19717422]
20. Fei J, et al. A highly purified, fluorescently labeled in vitro translation system for single-molecule studies of protein synthesis. Methods Enzymol. 2010; 472:221–59. [PubMed: 20580967]
21. Fei J, Kosuri P, MacDougall DD, Gonzalez RL Jr. Coupling of ribosomal L1 stalk and tRNA dynamics during translation elongation. Mol Cell. 2008; 30:348–59. [PubMed: 18471980]
22. Blanchard SC, Kim HD, Gonzalez RL Jr, Puglisi JD, Chu S. tRNA dynamics on the ribosome during translation. Proc Natl Acad Sci U S A. 2004; 101:12893–8. [PubMed: 15317937]
23. Sternberg SH, Fei J, Prywes N, McGrath KA, Gonzalez RL Jr. Translation factors direct intrinsic ribosome dynamics during translation termination and ribosome recycling. Nat Struct Mol Biol. 2009; 16:861–8. [PubMed: 19597483]
24. Bronson JE, Fei J, Hofman JM, Gonzalez RL Jr, Wiggins CH. Learning rates and states from biophysical time series: a Bayesian approach to model selection and single-molecule FRET data. Biophys J. 2009; 97:3196–205. [PubMed: 20006957]

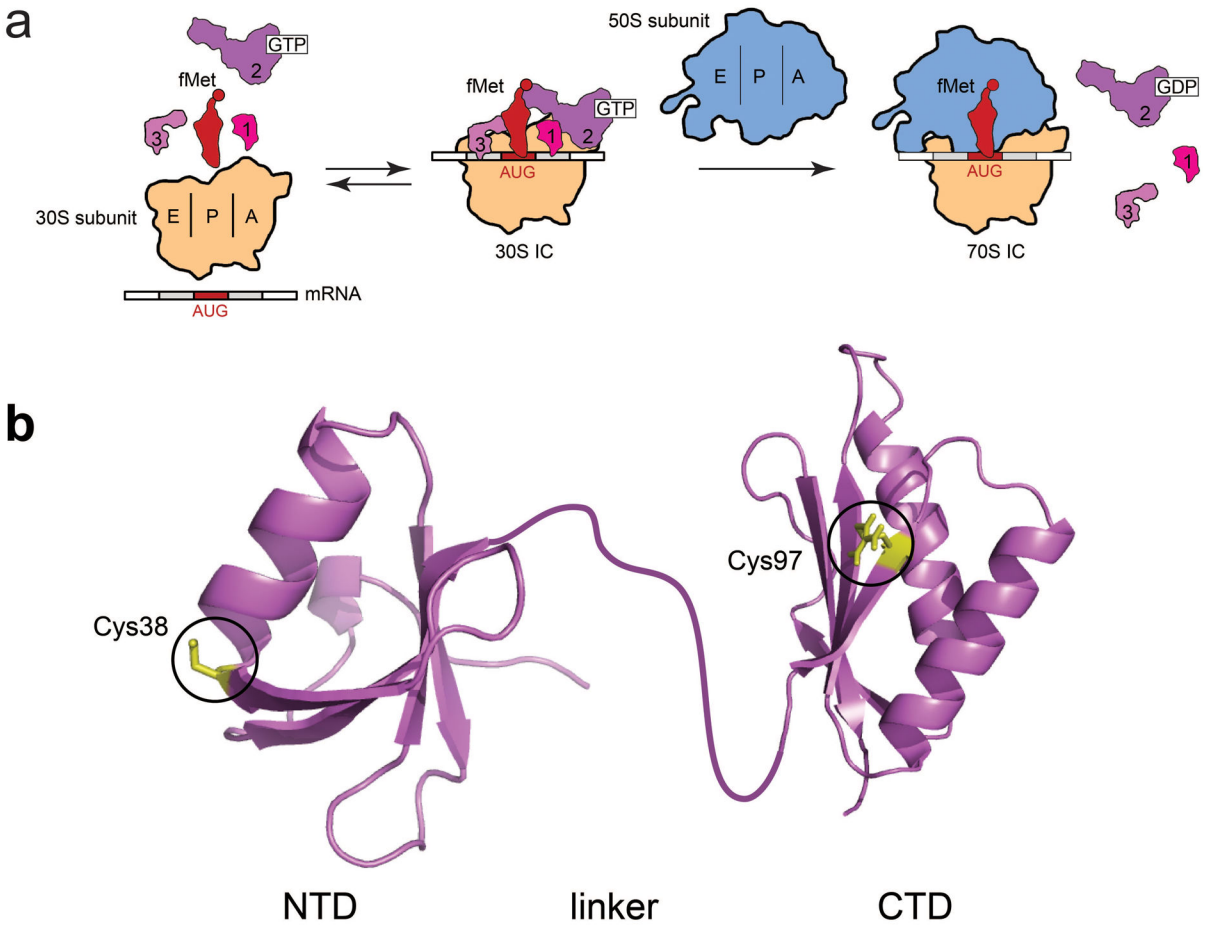

Figure 1.

Translation initiation in bacteria and fluorescent labeling of IF3. **(a)** A minimal model of translation initiation. "30S IC" refers to a completely and correctly assembled 30S ribosomal initiation complex; "70S IC" refers to a 70S ribosomal initiation complex harboring an initiator fMet-tRNA^{fMet} bound to an AUG start codon at the P site. The IFs, mRNA, and fMet-tRNA^{fMet} reversibly bind to the 30S ribosomal subunit to form the 30S IC[17]. Subsequent joining of the 50S subunit to the 30S IC triggers GTP hydrolysis by IF2, and, ultimately, dissociation of the three IFs. **(b)** X-ray crystal structures of the NTD (PDB ID: 1TIF) and CTD (PDB ID: 1TIG) of IF3 from *Bacillus stearothermophilus*. The linker connecting the NTD and CTD was cartooned by hand. A C65S, S38C, and K97C triple mutant of *E. coli* IF3 was prepared and fluorescently labeled with Cy3 and Cy5 at Cys38 and Cys97. The corresponding residues on the *B. stearothermophilus* structures are indicated in the depicted structure.

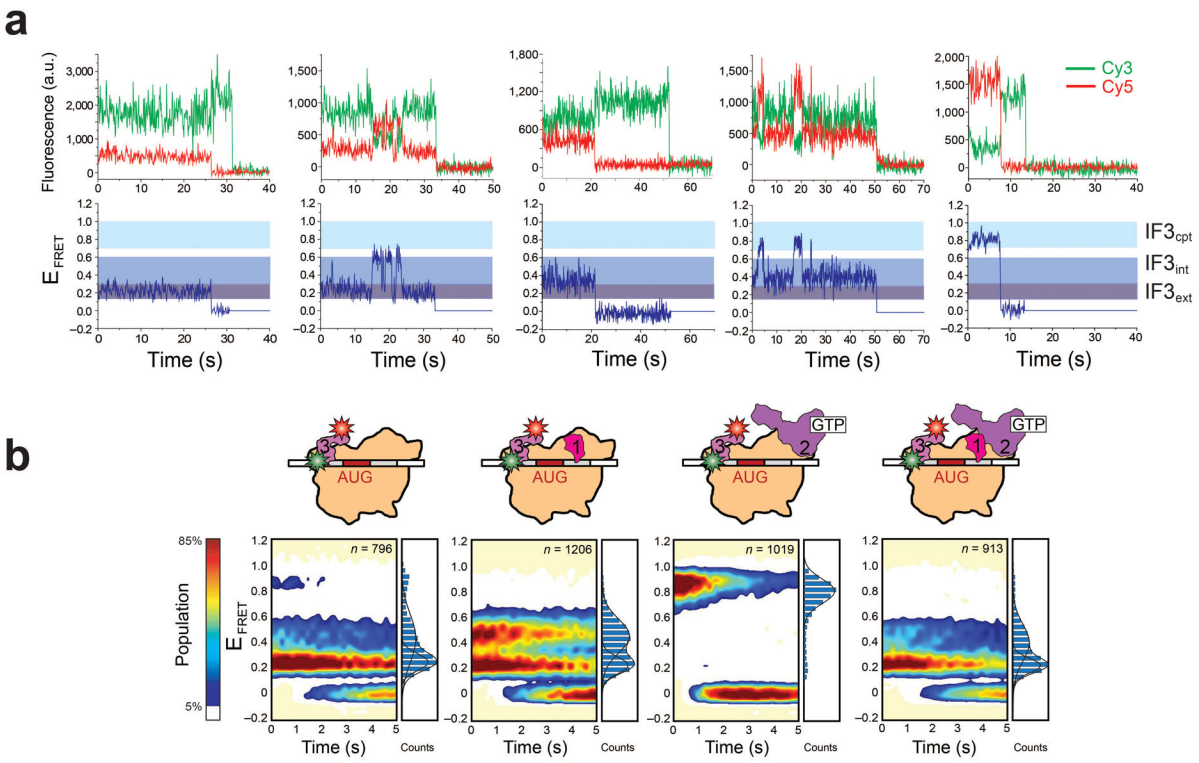

Figure 2.

smFRET measurements of $30S\,IC_{-1/-2}^{-tRNA}$, $30S\,IC_{-2}^{-tRNA}$, $30S\,IC_{-1}^{-tRNA}$, and $30S\ IC^{-tRNA}$. **(a)** Representative examples of single-molecule Cy3 (green lines)- and Cy5 (red lines) intensity *versus* time trajectories (top plot) and E_{FRET} (blue lines) *versus* time trajectories (bottom plot) for $30S\,IC_{-1/-2}^{-tRNA}$. "$IF3_{ext}$," "$IF3_{int}$," and "$IF3_{cpt}$" refer to the extended, intermediate, and compact conformations of IF3 that we assign to the FRET states centered at E_{FRET} values of 0.23 ± 0.01, 0.42 ± 0.01, and 0.87 ± 0.01, respectively. The trajectories depicted in the first, third, and fifth columns are examples of trajectories that sample only the $IF3_{ext}$, $IF3_{int}$, or $IF3_{cpt}$ conformations of IF3, respectively, prior to photobleaching. The trajectories depicted in the second and fourth columns are examples of trajectories that exhibit fluctuations between the $IF3_{ext}$ and $IF3_{int}$ conformations of IF3 and the $IF3_{int}$ and $IF3_{cpt}$ conformations of IF3, respectively, prior to photobleaching. **(b)** Two-dimensional surface contour plots of the time evolution of population FRET for $30S\,IC_{-1/-2}^{-tRNA}$, $30S\,IC_{-2}^{-tRNA}$, $30S\,IC_{-1}^{-tRNA}$, and $30S\ IC^{-tRNA}$. "*n*" represents the total number of E_{FRET} *versus* time trajectories that were used to construct each histogram. To the right of each contour plot is a normalized one-dimensional E_{FRET} histogram for the first 0.5 seconds of the E_{FRET} *versus* time trajectories comprising each dataset. The cartoon above each surface contour plot and E_{FRET} histogram depicts the composition of the 30S IC corresponding to the surface contour plot and E_{FRET} histogram.

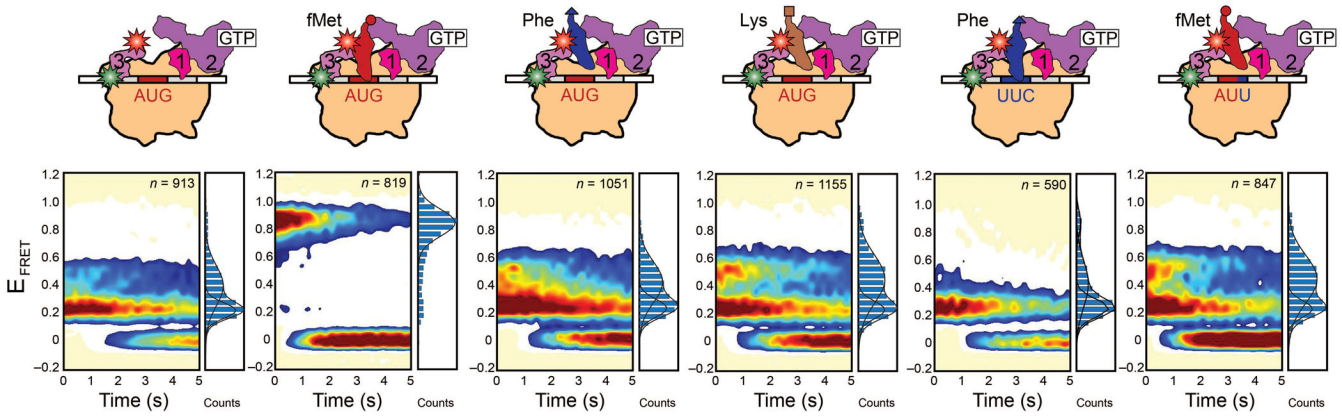

Figure 3.

smFRET measurements of 30S IC^{-tRNA}, 30S IC^{fMet}, 30S IC^{Phe}, 30S IC^{Lys}, 30S IC^{Phe,UUC}, and30S IC^{fMet,AUU}. Data are displayed as in Fig. 2B.

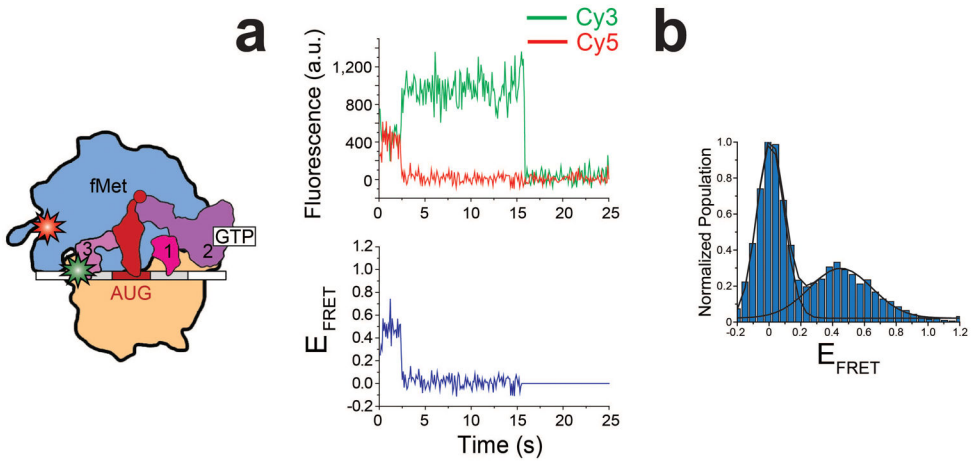

Figure 4. Observation of an intermolecular IF3-50S subunit smFRET signal

Stopped-flow delivery of a solution containing 50 nM Cy5-labeled 50S subunit (labeled at $L9_{Q18C}$ as previously described)[19] into a flowcell containing a surface-tethered 30S IC^{fMet} carrying $IF3_{C65S\ S38C}$(Cy3) results in an intermolecular IF3-50S subunit smFRET signal that reports on 50S subunit joining and formation of a 70S ribosomal initiation complex (70S IC). The cartoon depicts the 70S IC that is formed during the stopped-flow experiment. **(a)** A representative example of a single-molecule Cy3 (green line)- and Cy5 (red line) intensity *versus* time trajectory (top plot) and E_{FRET} *versus* time trajectory (bottom plot) for the 70S IC. **(b)** A normalized, one-dimensional E_{FRET} histogram for the full 120 seconds of the E_{FRET} *versus* time trajectories (n = 25). The FRET state centered at an E_{FRET} value of ~0.45 arises from time points in the E_{FRET} *versus* time trajectories during which the Cy5-labeled 50S subunit has joined to a 30S IC carrying the Cy3-labeled IF3. The FRET state centered at an E_{FRET} value of ~0 arises from time points in the E_{FRET} *versus* time trajectories prior to joining of the Cy5-labeled 50S subunit to the 30S IC carrying the Cy3-labeled IF3 and from time points subsequent to photobleaching of Cy5 on the Cy5-labeled 50S subunits.

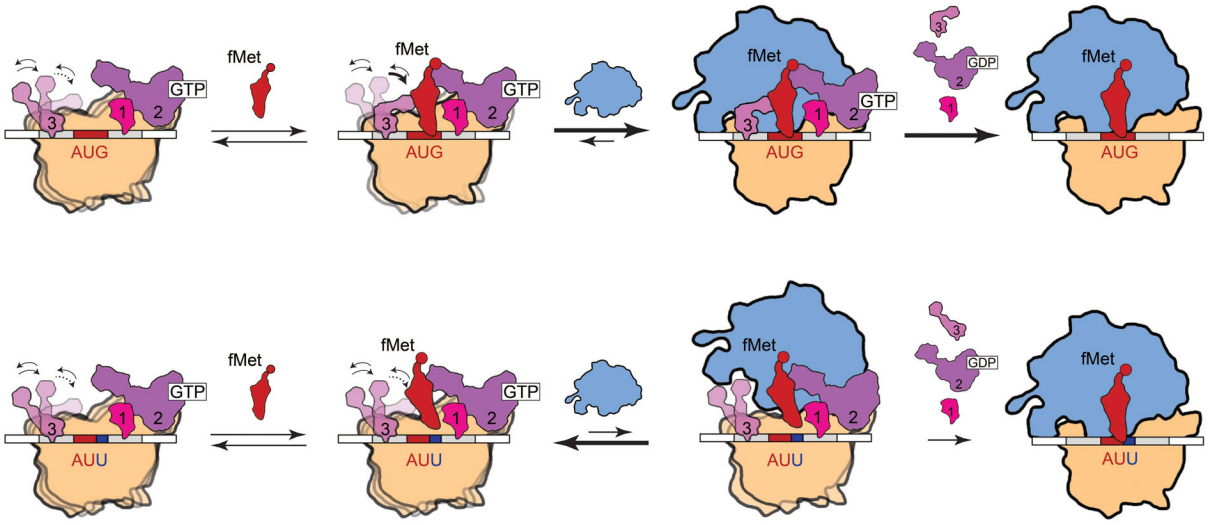

Figure 5.

A structure-based mechanistic model for how IF3 recognizes and signals fMet-tRNA^{fMet} and start codon selection within the 30S IC. 30S IC-bound IF3 exists in a conformational equilibrium in which it can dynamically exchange between at least three distinct conformational states, IF3$_{ext}$, IF3$_{int}$, and IF3$_{cpt}$. Specific recognition of an fMet-tRNA^{fMet} that is properly base paired to a start codon within the P site of a 30S IC carrying all three IFs strongly shifts the conformational equilibrium of IF3 towards IF3$_{cpt}$, a conformation of 30S IC-bound IF3 that exposes and/or optimally positions ribosomal RNA and/or ribosomal protein residues on the 30S IC that are critical for intersubunit bridge formation and is thus conducive to rapid and productive 50S subunit joining (top row). In contrast, the absence of an aa-tRNA, the presence of an elongator aa-tRNA, or the presence of a non-canonical start codon within the P site of a 30S IC carrying all three IFs strongly shifts the conformational equilibrium of IF3 towards IF3$_{ext}$ and IF3$_{int}$, conformations of 30S IC-bound IF3 that occlude and/or misorient residues involved in intersubunit bridge formation and are thus not conducive to efficient 50S subunit joining (bottom row).